analytical chemistry

pubs.acs.org/ac Article

Peptide-Based Photocathodic Biosensors: Integrating a Recognition Peptide with an Antifouling Peptide

Shiting Gu,[§] Xiao-Mei Shi,[§] Di Zhang, Gao-Chao Fan,* and Xiliang Luo*

Cite This: *Anal. Chem.* 2021, 93, 2706−2712 Read Online

ACCESS | Metrics & More | Article Recommendations | Supporting Information

ABSTRACT: Accurate and sensitive detection of targets in practical biological matrixes such as blood, plasma, serum, or tissue fluid is a frontier issue for most biosensors since the coexistence of both potential reducing agents and protein molecules has the possibility of causing signal interference. Herein, aiming at detection in a complex environment, an advanced and robust peptide-based photocathodic biosensor, which integrated a recognition peptide with an antifouling peptide in one probe electrode, was first proposed. Selecting human chorionic gonadotropin (hCG) as a model target, the recognition peptide with the sequence PPLRINRHILTR was first anchored on the $CuBi_2O_4$/Au (CBO/Au) photocathode and then the antifouling peptide with the sequence EKEKE-KEPPPPC was further anchored to generate an antifouling biointerface. The peptide-based photocathodic biosensor demonstrated excellent anti-interference to both nonspecific proteins and reducing agents because of the capability of the antifouling peptide. It also exhibited good sensitivity owing to the utilization of the recognition peptide rather than an antibody probe. This peptide-integrated method offers a new perspective for practical applications of photocathodic biosensors.

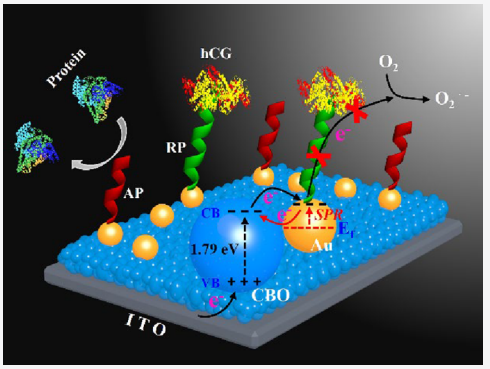

INTRODUCTION

As an important means to diagnose major diseases such as common cancers, various advanced biosensors have received widespread attention. However, there are several other potential reducing agents and protein molecules in addition to the target to detect in real biological samples,[1−4] which very easily foul the biosensor interface. As a result, the reliability of the detection results usually has been greatly restricted, causing a challenge for accurate diagnosis of major diseases. Photoelectrochemical (PEC) biosensors have aroused great attention in recent years benefiting from their distinct merits of simple equipment, easy operation, low cost, low background noise, and high sensibility.[5−7] PEC biosensors can be classified into photoanodic and photocathodic ones based on the nature of the photoelectrode involved.[8,9] It has been demonstrated that the photocathodic biosensors built on a p-type photoelectrode present a much better anti-interference ability to reducing agents than the photoanodic biosensors built on a n-type photoelectrode,[10−13] showing the prospects for practical applications. Unfortunately, the pursuit for robust photocathodic biosensors capable of sensitive and accurate detection in complex biological media is still in the initial phase and leaves much to be desired.

Peptides are formed from natural amino acids. There are many promising applications of novel peptides such as tissue engineering, enzyme mimics, and biomaterial development,[14−17] owing to their remarkable characteristics of biological simplicity, structural stability, easy synthesis, and low cost for short peptides. Toward biosensors, the role of short peptides mainly involves recognition and antifouling. Recognition peptides, namely, peptide aptamers, are considered as more prospective probe molecules to replace antibodies in the area of biosensors.[18−20] Recognition peptides originate from the same amino acids that constitute proteins and could mimic protein interactions, which allow them to bind to the specific target with high affinity and specificity.[18−20] In addition, short recognition peptides exhibit small steric hindrance, which could decrease the signal loss and increase the initial response of the biosensor effectively, and hence enhance the sensitivity. On the other hand, antifouling peptides exist as zwitterions at isoelectric points and exhibit electric neutrality.[21,22] They can form a strong hydration layer like a uniform and dense brush at the biointerface to prevent the adhesion of nonspecific proteins.[22−24] However, to best of our knowledge, peptide-based photocathodic biosensors, either with recognition peptides or with antifouling peptides or even with both of them, have not been reported yet despite the powerful advantages of these functional peptides.

Received: December 14, 2020
Accepted: December 29, 2020
Published: January 11, 2021

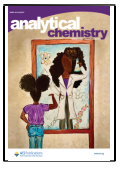

https://dx.doi.org/10.1021/acs.analchem.0c05234
Anal. Chem. 2021, 93, 2706−2712

Scheme 1. Construction of the Peptide-Based Photocathodic Biosensor Integrating a Recognition Peptide with an Antifouling Peptide

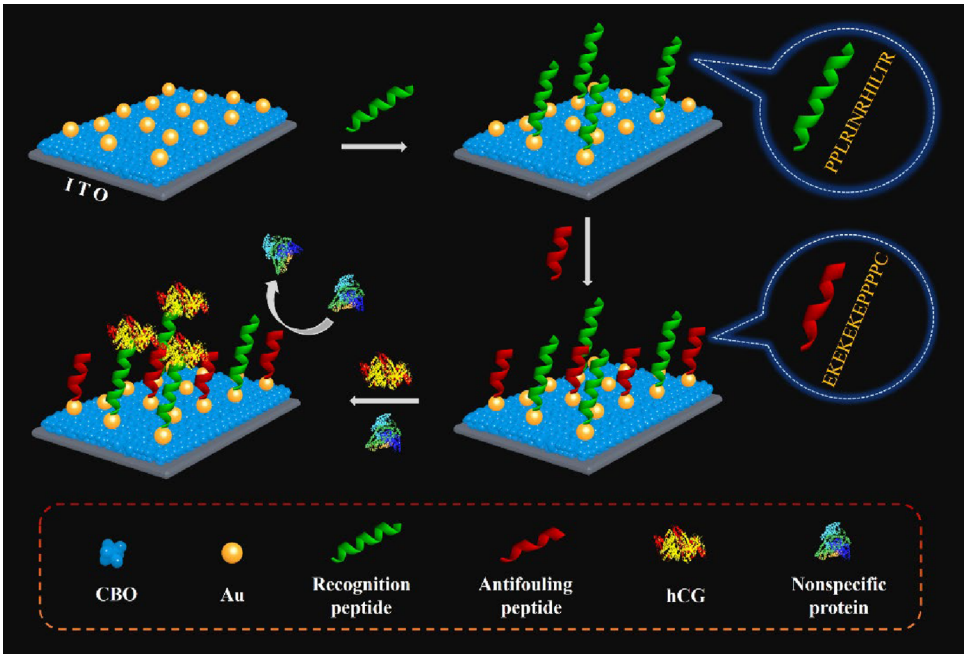

Inspired by the plight above, we designed herein a simple but feasible peptide-based photocathodic biosensor, as shown in Scheme 1. The salient feature of the photocathodic biosensor is the integration of a recognition peptide with an antifouling peptide in one probe electrode, which endowed the biosensor with high sensitivity and good selectivity for real sample detection. Human chorionic gonadotropin (hCG), an important biomarker for pregnancy and several cancers,[25,26] was selected as a model target for detection. After deposition of a $CuBi_2O_4$ (CBO) layer and then decoration of Au nanoparticles (NPs) on an indium tin oxide (ITO) substrate, the CBO/Au photocathode was prepared. The recognition peptide for the target hCG with the sequence PPLRINRHILTR was first anchored on the CBO/Au photocathode via bonding of NH_2−Au. The antifouling peptide with the sequence EKEKEKEPPPPC was then anchored via a S−Au bond to form an antifouling interface of the biosensor. The target hCG was finally detected by the remarkable decrease in the photocurrent signal resulting from the large steric hindrance of the recognized glycoprotein hCG.

EXPERIMENTAL SECTION

Materials and Reagents. Bismuth nitrate ($Bi(NO_3)_3$), ethylene glycol, glucose (Glu), glutathione (GSH), ascorbic acid (AA), chloroauric acid ($HAuCl_4$), sodium hydroxide (NaOH), and copper nitrate ($Cu(NO_3)_2$) were purchased from Sigma-Aldrich (USA).ITO substrates were obtained from Zhuhai Kaivo Optoelectronic Technology Co., Ltd. (China). Bovine serum albumin (BSA), myoglobin (Mb), human serum albumin (HSA), and human immunoglobulin G (HIgG) were obtained from Wuhan USCN Life Science Inc. (China). The target hCG was offered by Shanghai Yuduo Biotechnology Co. Ltd. (China).

The peptides used were synthesized by Hefei Bankpeptide Biological Technology Co. Ltd. (China) with the following sequences:

Recognition peptide: PPLRINRHILTR, where P, L, R, I, N, H, and T represent proline, leucine, arginine, isoleucine, asparagine, histidine, and threonine, respectively. The molecule structure is shown in Figure S1.

Antifouling peptide: EKEKEKEPPPPC, where K, E, C, and P represent lysine, glutamic acid, cysteine, and proline, respectively. The molecule structure is shown in Figure S2.

Phosphate buffer solution (PBS, 10 mM, pH 7.4) served as the solvent for the preparation of peptide solutions.

The apparatus employed for characterizations and PEC measurement is described in detail in the Supporting Information.

Preparation of the CBO/Au Photocathode. A CBO film was first fabricated on an ITO electrode using the potentiostatic method.[27] The electrolyte solution was ethylene glycol dissolved with 100 mM $Bi(NO_3)_3$ and 30 mM $Cu(NO_3)_2$. The deposition process was conducted for a period of 60 s under a steady potential E = −1.8 V versus Hg/Hg_2Cl_2. After treatment at 450 °C in an air atmosphere for 3 h, the desired CBO electrode was obtained. The decoration of Au NPs on the fabricated CBO electrode was based on a method reported in the literature.[28] Typically, 10 mM $HAuCl_4$ aqueous solution was first regulated to pH 4.5 with a NaOH solution. The CBO electrode was then incubated with 10 μL of this $HAuCl_4$ solution for 30 min at an ambient temperature. After rinsing with deionized water, the CBO/Au photocathode was obtained finally after calcination at 300 °C for 2 h in an air atmosphere.

Fabrication of the Peptide-Based Biosensor. Typically, the CBO/Au photocathode was incubated first with 20 μL of 0.2 mg/mL recognition peptide solution at 4 °C for 8 h under humid conditions. Then, the electrode was rinsed gently with PBS (10 mM, pH 7.4) and was further incubated with 20 μL of 0.2 mg/mL antifouling peptide solution at 4 °C under humid conditions for another 6 h to form an antifouling biointerface. After rinsing gently with PBS, the resulting electrode acted as a biosensor and was incubated with 20 μL of different

https://dx.doi.org/10.1021/acs.analchem.0c05234
Anal. Chem. 2021, 93, 2706−2712

concentrations of hCG at 37 °C for 1 h. After PBS rinsing, the electrode was prepared for PEC detection.

RESULTS AND DISCUSSION

Design Principle. The PEC mechanism of the peptide-based photocathodic biosensor is illustrated in Scheme 2. The CBO/Au photocathode acted as the signal conversion element to generate an evident and stable cathodic photocurrent. CBO is a nontoxic p-type ternary compound semiconductor with a narrow band gap of 1.79 eV (the calculation of the band gap value is shown in Figure S3), which enables it to effectively absorb the visible light spectrum.[29,30] Noble metal Au NPs have been demonstrated to exhibit excellent electron conductivity and optical characteristics due to their surface plasmon resonance (SPR) effect. The plasmon-excited hot electrons at the surface of the Au NPs could be injected to the conduction band of the semiconductor contact and strongly couple with the photogenerated electrons of the semiconductor, which effectively extends the lifetime of the excited electrons.[31−34] Hence, combining Au NPs with CBO to form a CBO/Au photocathode could significantly diminish charge recombination in CBO and generate an evident cathodic photocurrent output.

The peptide with the sequence PPLRINRHILTR served as the recognition element that had a strong specific affinity with the target hCG.[35,36] The short recognition peptide exhibited a much smaller steric hindrance than the antibody probe used traditionally,[37,38] which obviously reduced the loss of the photocurrent output of the CBO/Au photocathode, contributing to sensitivity enhancement. The peptide with the sequence EKEKEKEPPPPC served as the antifouling element that had good capability to resist nonspecific absorption of proteins at the biointerface.[39,40] The alternate EK segment with opposite charges was the antifouling domain,[39] while the PPPPC segment was a useful linker for surface anchoring.[40] Compared with traditional blocking reagents such as BSA, the antifouling peptide exhibits the desired merits of small steric hindrance and enhanced antifouling properties for surface blocking. After the peptide-based photocathodic biosensor was incubated with target hCG, the large steric hindrance generated by specific binding with glycoprotein hCG remarkably hindered the excitation electrons at the photocathode interface from being captured by the electron acceptor of dissolved O_2, causing an evident decrease in the photocurrent detection signal. Thus, the sensitive and accurate detection of target hCG in a complex biological matrix could be achieved.

Scheme 2. PEC Mechanism of the Peptide-Based Photocathodic Biosensor for Target hCG Detection[a]

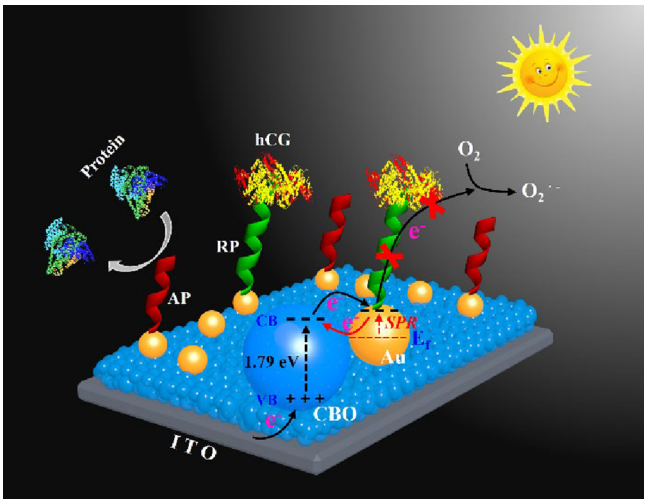

[a]Note: RP and AP in the scheme stand for recognition peptide and antifouling peptide, respectively.

Characterization of the Photocathode. The fabrication of the CBO/Au photocathode was first observed by scanning electron microscopy (SEM). As shown in Figure 1A, the CBO electrode was fully covered by an interconnected structure with abundant smooth particles of size of 90−120 nm as ingredients. After Au NP decoration, as shown in Figure 1B, many small NPs with a size of 35 ± 5 nm distributed uniformly on the surface of the CBO electrode. In addition, the elemental mapping shown in the inset of Figure 1A,B also indicated the formation of the CBO/Au photocathode.

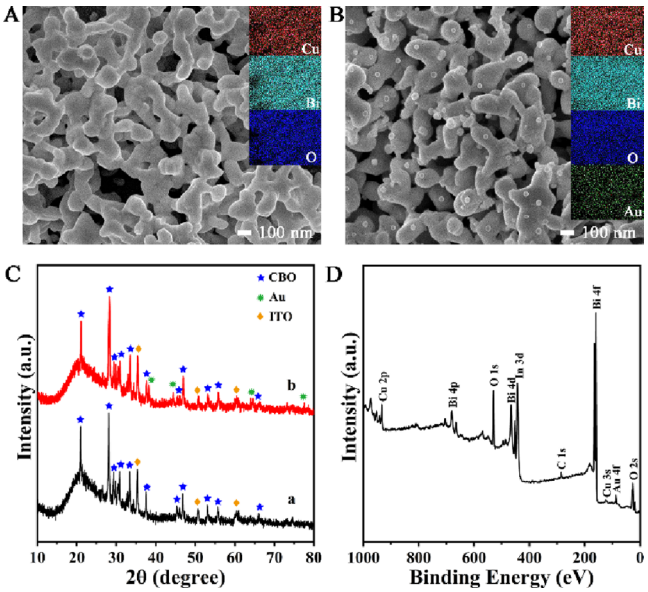

Figure 1. SEM images of (A) CBO and (B) CBO/Au electrodes; (C) XRD patterns of the CBO (curve a) and CBO/Au (curve b) electrodes; and (D) XPS full-scan spectrum of the CBO/Au electrode. The insets in panels A and B show the elemental mapping of (Cu, Bi, and O) and (Cu, Bi, O, and Au).

Powder X-ray diffraction (XRD) was then further employed to characterize the CBO/Au photocathode, as shown in Figure 1C. Curve a shows the typical XRD pattern of the CBO electrode. The specific diffraction peaks observed at 2θ = 20.83, 28.11, 33.36, 37.51, 46.82, 53.09, and 55.7° could be well assigned to the (200), (211), (310), (202), (411), (213), and (332) crystal planes of the pure CBO phase (PDF no. 48−1886). Inevitably, the other diffraction peaks at 2θ = 35.3, 50.84, and 60.03° were all attributed to the pure ITO phase from the ITO substrate. After Au NP decoration, the characteristic diffraction peaks in curve b observed at 2θ = 38.14, 44.34, 64.56, and 77.38° were indexed to the (111), (200), (220), and (311) crystal planes of Au (PDF no. 65−2870), proving the successful decoration of Au NPs on the CBO electrode.

X-ray photoelectron spectroscopy (XPS) was also used to characterize the chemical composite and the valence state of the CBO/Au photocathode. Figure 1D shows the XPS full-

https://dx.doi.org/10.1021/acs.analchem.0c05234
Anal. Chem. 2021, 93, 2706−2712

scan spectrum of the CBO/Au photocathode. The XPS characteristic peaks of Cu 2p, Bi 4p, O 1s, Bi 4d, Bi 4f, Cu 3s, and O 2s originated from CBO, while the characteristic peak of Au 4f was from the decorated Au NPs and In 3d was from the ITO matrix. The C 1s peak was adopted as an internal reference to calibrate the binding energy. In addition, the XPS high-resolution spectra of Cu 2p, Bi 4f, O 1s, and Au 4f for the CBO/Au photocathode are shown in Figure S4, which further verified the successful fabrication of the CBO/Au photocathode.

XPS Characterization of Peptide Anchoring. To verify the modifications of the recognition peptide and the antifouling peptide on the surface of the CBO/Au photocathode, XPS full-scan spectra were used to inspect the variation of the chemical elements. After recognition peptide anchoring, as shown in Figure 2A, a new characteristic peak for

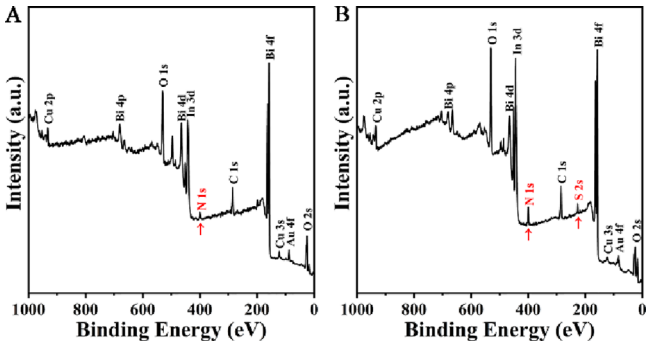

Figure 2. XPS spectra of the CBO/Au photocathode modified with (A) recognition peptide and then (B) antifouling peptide.

N 1s appeared at 399.8 eV compared with the previous CBO/Au photocathode, which is attributed to a characteristic element of the recognition peptide. After further blocking the biointerface with the antifouling peptide, as shown in Figure 2B, the peak intensity for N 1s enhanced obviously and meanwhile another new characteristic peak for S 2s emerged at 226.7 eV, attributed to a characteristic element of the antifouling peptide. The XPS spectra hence clearly confirmed the successful anchoring of both the recognition peptide and the antifouling peptide on the CBO/Au photocathode.

Characterization of the Peptide-Based Biosensor. The fabricated peptide-based photocathodic biosensor was characterized first by the photocurrent output, as shown in Figure 3A.

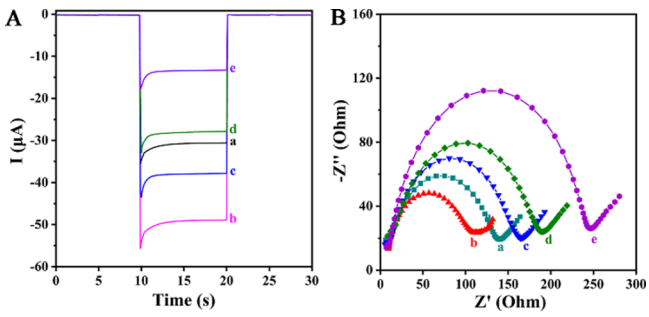

Figure 3. (A) Photocurrent outputs and (B) electrochemical impedance spectroscopy (EIS) curves of (a) the CBO electrode, (b) after Au NP decoration, (c) after recognition peptide anchoring, (d) after antifouling peptide anchoring, and (e) after further incubation with hCG.

Under the optimal conditions, a moderate output of the cathodic photocurrent was measured for the CBO electrode (curve a) since CBO with a narrow band gap of 1.79 eV can achieve effective absorption of the visible light. After Au NP decoration, the output of the cathodic photocurrent enhanced evidently (curve b) because the SPR effect of the Au NPs inhibited charge recombination and increased the total charge density available. In addition, the stability of the CBO/Au photocathode was studied from the time-varied photocurrent output, as shown in Figure S5, and a satisfactory result was obtained. After stepwise anchoring of the recognition peptide and the antifouling peptide on the photocathode (curves c and d), a continuous decrease in the cathodic photocurrent was observed due to the weak charge-transfer abilities of the peptides. After the biosensor underwent target hCG incubation (curve e), the cathodic photocurrent signal weakened notably, owing to the evident steric hindrance of the glycoprotein hCG. The expected variation trend of the cathodic photocurrent demonstrated successful development of the peptide-based photocathodic biosensor.

EIS was then employed for inspecting the fabricated peptide-based biosensor, as shown in Figure 3B. The electron-transfer resistance (R_{et}) is represented by the semicircle diameter of the curve. The CBO electrode showed a moderate R_{et} value (curve a). After Au NP decoration, the R_{et} diminished obviously (curve b) because of the excellent electron conductivity of Au NPs. With successive anchoring of the recognition peptide and the antifouling peptide (curves c and d), the R_{et} increased gradually owing to the poor conductivity of the peptides. After the biosensor was incubated with target hCG, the R_{et} increased markedly (curve e), confirming the specific binding affinity of the recognition peptide with hCG. The EIS variation thus also suggested the successful fabrication of the peptide-based biosensor.

Optimal Conditions for the Biosensor. To obtain better detection performance, some important parameters and conditions were optimized. Figure 4A shows the photocurrent output of the CBO electrode with extended deposition times. It is observed that a deposition time of 60 s for CBO modification corresponds to the peak value of the cathodic photocurrent. With the extension of the deposition time initially, the amount of CBO on the electrode gradually accumulated and the photocurrent output enhanced accordingly. However, the photocurrent output was found to reduce as the time for deposition was increased beyond 60 s, resulting from the obvious cumulative diffusion resistance for electron motion. Hence, a deposition time of 60 s was selected for the CBO electrode.

Figure 4B shows the photocurrent output of the CBO/Au photocathode incubated with varied concentrations of $HAuCl_4$. As shown, the photocathode incubated with 10 mM $HAuCl_4$ showed the highest photocurrent output. In the beginning, the increased incubation concentration of $HAuCl_4$ could yield more Au NPs to offer hot electrons and inhibit charge recombination, whereas the excessive amount of Au NPs produced by the high incubation concentration of $HAuCl_4$ would inevitably cause electron annihilation due to the increased distance for electron transmission.

Figure 4C shows the photocurrent output of the electrode modified with the recognition peptide of different incubation concentrations. As the incubation concentration of the recognition peptide increased, the cathodic photocurrent gradually decreased and then nearly approached a plateau

https://dx.doi.org/10.1021/acs.analchem.0c05234
Anal. Chem. 2021, 93, 2706−2712

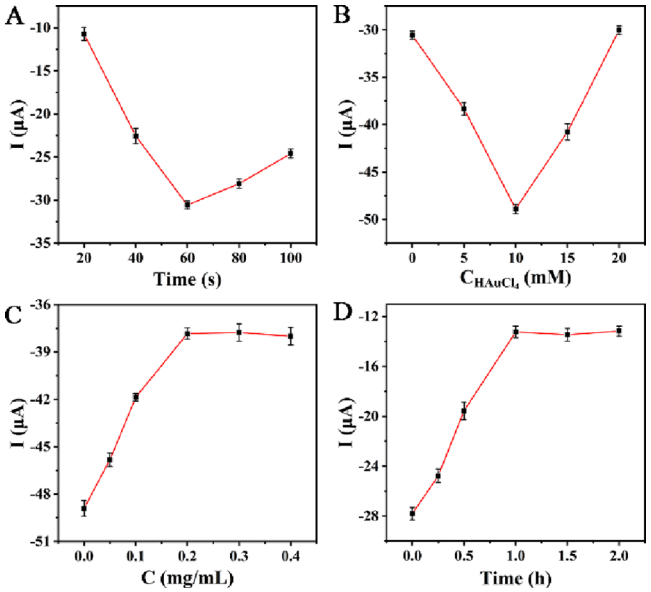

Figure 4. Photocurrent outputs of (A) the CBO electrode with extended deposition times, (B) the CBO/Au electrode incubated with varied concentrations of $HAuCl_4$, (C) the recognition peptide-modified electrode with varied incubation concentrations, and (D) the peptide-based cathodic biosensor with different incubation times of target hCG.

when the incubation concentration reached 0.2 mg/mL, indicating that adequate bioprobes were anchored on the electrode. As a result, 0.2 mg/mL was chosen as the incubation concentration of the recognition peptide.

Figure 4D shows the photocurrent output of the peptide-based cathodic biosensor with varied incubation times of target hCG. With the extension of the incubation time, as shown, the cathodic photocurrent gradually weakened due to the specific affinity of the recognition peptide with hCG, and subsequently, the cathodic photocurrent signal almost reached a plateau at approximately 1 h. Thus, the incubation time of target hCG was selected as 1 h.

Antifouling Property of the Biosensor. Nonspecific adsorption is a great issue for biosensors employed in practical biological matrixes. It is demonstrated that antifouling peptides with electric neutrality and good hydrophilicity can effectively resist the nonspecific biomolecule adsorption.[41,42] To inspect the features of the antifouling peptide, both zeta potential and static water contact angle were measured. Figure S6 shows the zeta potential of the antifouling peptide dissolved in deionized water (1.0 mg/mL solution for test), which was approximately 0.0 mV, indicating electric neutrality of the peptide. The hydrophilicity of the peptide-based biointerface was assessed by static water contact angle measurements, as shown in Figure S7. The CBO/Au photocathode showed a contact angle of 34.6°, and after anchoring of the recognition peptide and the antifouling peptide in order, the contact angles reduced to 19.2 and 13.5°, respectively. The measurement of the water contact angle thus indicated that the antifouling peptide-modified biointerface exhibited excellent hydrophilicity, which has a latent capacity for antifouling performance.

The antifouling performance of the peptide-based biosensor was further verified by fluorescence microscopy. As clearly shown in Figure 5A,B, plenty of labeled proteins of FITC−BSA adhered on the CBO/Au photocathode and that with recognition peptide anchoring. Conversely, the biosensor with

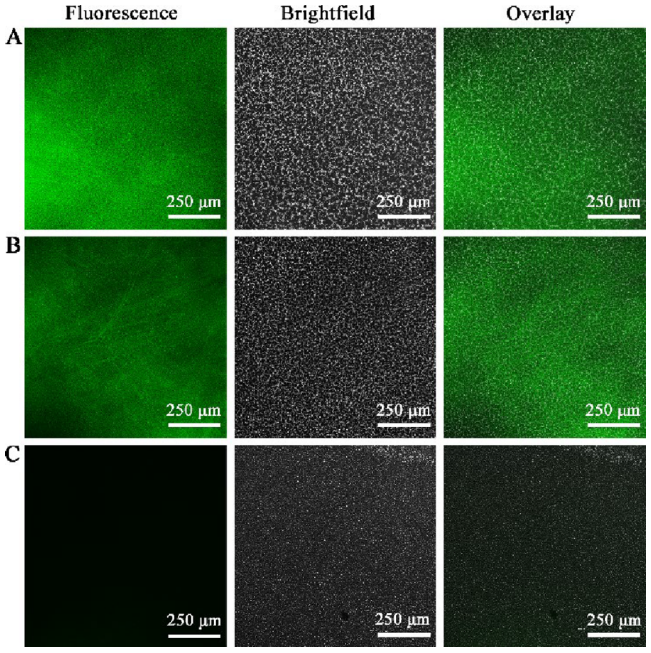

Figure 5. Fluorescence microscopy images of electrodes of CBO/Au (A), CBO/Au/RP (B), and CBO/Au/RP/AP after incubated with 2.0 mg/mL of fluorescein isothiocyanate-labeled BSA (FITC−BSA) for 2 h (RP and AP stand for recognition peptide and antifouling peptide, respectively).

antifouling peptide anchoring presented a relatively clean and tidy surface after being incubated with FITC−BSA for 2 h, as shown in Figure 5C. The result thus clearly confirmed that the designed peptide-based photocathodic biosensor possesses good antifouling ability to repel nonspecific protein adsorption.

Analytical Performances. The detection principle of target hCG was based on the photocurrent variation generated by the evident steric hindrance of the glycoprotein hCG when the specific binding affinity occurred. As shown in Figure 6A,

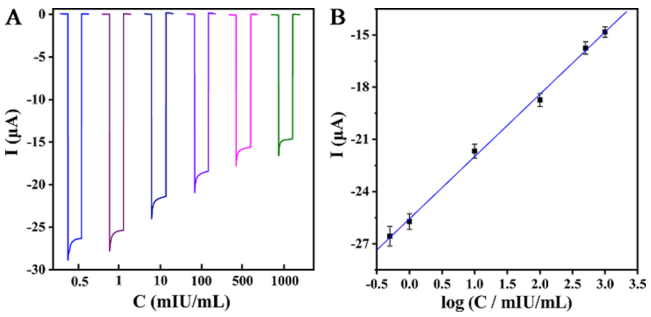

Figure 6. (A) Photocurrent signal and (B) calibration curve of the peptide-based photocathodic biosensor for different concentrations of target hCG detection.

the photocurrent response of the biosensor reduced accordingly with an increase in the hCG concentration, implying that more target molecules were captured by the recognition peptides. Figure 6B shows the calibration curve of the peptide-based photocathodic biosensor against a wide concentration range from 0.5 to 1000 mIU/mL of hCG. The linear regression equation was I = −25.56 + 3.58 log C (mIU/mL), with 0.9970 as its correlation coefficient. The limit of detection (LOD, S/N = 3) for target hCG was calculated to be 0.19 mIU/mL.

https://dx.doi.org/10.1021/acs.analchem.0c05234
Anal. Chem. 2021, 93, 2706−2712

Compared with sensitive hCG biosensors developed previously,[43−48] the fabricated peptide-based photocathodic biosensor had a comparable or even lower LOD.

To assess the antifouling capability of the photocathodic biosensor, the photocurrent outputs of the biosensor without and with antifouling peptide anchoring were tested while incubated in the biological media of human serum. As shown in Figure 7A, the biosensor with the antifouling peptide

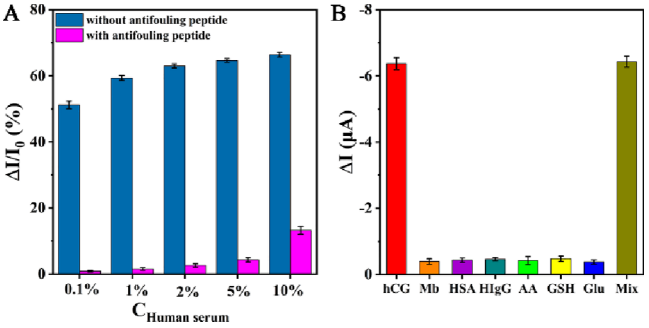

Figure 7. (A) Change in photocurrent responses ($\Delta I/I_0$) of the biosensor without or with the antifouling peptide while incubated in a diluted human serum. (B) Photocurrent changes of the biosensor to 10 mIU/mL of hCG, 0.1 ng/mL of Mb, HSA, HIgG, 10 mM GSH, AA, Glu, and all the mixture (Mix). $\Delta I = I_0 - I$; I_0 and I denote the photocurrent signal of the biosensor before (I_0) and after (I) incubation.

presented a much smaller photocurrent variation than that without antifouling peptide in human serum, and the biosensor with the antifouling peptide showed a good antifouling performance against the human serum even at a 5% diluted level (with the value of 4.3% as the photocurrent change rate). Hereby, the results verified the potential utility of the fabricated peptide-based cathodic biosensor in real biosamples.

In order to realize accurate detection in a complex environment, high selectivity is especially important for a biosensor. As potential substances like protein molecules and reducing agents are usually present in a biological matrix, some of them such as Mb, HSA, HIgG, AA, GSH, and Glu were selected to be added in a diluted human serum (2%) for the interference test. As shown in Figure 7B, both the interfering proteins and reducing agents exhibited negligible photocurrent changes compared to hCG detection. The result confirmed that the produced photocurrent signal was indeed generated from the target recognition and was unaffected by potential interfering substances, proving the good selectivity of the peptide-based photocathodic biosensor.

The repeatability of the biosensor was inspected by measuring five sensing electrodes fabricated individually. The photocurrent signals offered a relative standard deviation of 4.1% to 50 mIU/mL of hCG, indicating acceptable repeatability. The stability of the biosensor was investigated by the photocurrent change within the period of storage time. After 1 week of refrigerator storage, five sensing electrodes were incubated with 10 mIU/mL of hCG, and the photocurrent attenuations were all well within 5% compared with the freshly prepared sensing electrodes, reflecting favorable stability.

CONCLUSIONS

In summary, a new type of peptide-based photocathodic biosensor for sensitive and accurate analysis of targets in a complex biological matrix was developed. The CBO/Au photocathode presented a remarkable photocurrent output and favorable stability, being qualified as a cathodic matrix to anchor subsequent peptides. A short peptide instead of a high sterically hindered antibody was used as the recognition element, which evidently enhanced the sensitivity. Meanwhile, the antifouling peptide acted as an interfacial brush to resist the nonspecific adsorption of other reducing agents and protein molecules, which obviously avoided signal interference from the complex environment and promoted selectivity. Such a peptide-integrated photocathodic biosensing system provides a promising means for the fabrication of other advanced photocathodic bioassays capable of being used in practical applications.

ASSOCIATED CONTENT

Supporting Information

The Supporting Information is available free of charge at https://pubs.acs.org/doi/10.1021/acs.analchem.0c05234.

Structures of the recognition peptide and the antifouling peptide, apparatus employed, PEC measurement, band gap calculation of CBO, high-resolution XPS spectra of the photocathode, stability of the photocathode, zeta potential of the antifouling peptide, and static water contact angles of the electrodes (PDF)

AUTHOR INFORMATION

Corresponding Authors

Gao-Chao Fan − *Shandong Key Laboratory of Biochemical Analysis, College of Chemistry and Molecular Engineering, Qingdao University of Science and Technology, Qingdao 266042, China;* orcid.org/0000-0002-4645-3115; Email: gcfan@qust.edu.cn

Xiliang Luo − *Shandong Key Laboratory of Biochemical Analysis, College of Chemistry and Molecular Engineering, Qingdao University of Science and Technology, Qingdao 266042, China;* orcid.org/0000-0001-6075-7089; Email: xiliangluo@qust.edu.cn

Authors

Shiting Gu − *Shandong Key Laboratory of Biochemical Analysis, College of Chemistry and Molecular Engineering, Qingdao University of Science and Technology, Qingdao 266042, China*

Xiao-Mei Shi − *State Key Laboratory of Analytical Chemistry for Life Science, School of Chemistry and Chemical Engineering, Nanjing University, Nanjing 210093, China*

Di Zhang − *Shandong Key Laboratory of Biochemical Analysis, College of Chemistry and Molecular Engineering, Qingdao University of Science and Technology, Qingdao 266042, China*

Complete contact information is available at: https://pubs.acs.org/10.1021/acs.analchem.0c05234

Author Contributions

§S.G. and X.M.S. contributed equally to this work.

Notes

The authors declare no competing financial interest.

ACKNOWLEDGMENTS

This work is supported by the National Natural Science Foundation of China (22074073 and 21275087), the Taishan

Scholar Program of Shandong Province of China (ts20110829), and the Open Project Program of Key Laboratory for Analytical Science of Food Safety and Biology, Ministry of Education.

REFERENCES

(1) Banerjee, I.; Pangule, R. C.; Kane, R. S. *Adv. Mater.* **2011**, *23*, 690−718.
(2) He, M.; Gao, K.; Zhou, L.; Jiao, Z.; Wu, M.; Cao, J.; You, X.; Cai, Z.; Su, Y.; Jiang, Z. *Acta Biomater.* **2016**, *40*, 142−152.
(3) Qian, Q.; Deng, J.; Wang, D.; Yang, L.; Yu, P.; Mao, L. *Anal. Chem.* **2012**, *84*, 9579−9584.
(4) Xu, Y. T.; Yu, S. Y.; Zhu, Y. C.; Fan, G. C.; Han, D. M.; Qu, P.; Zhao, W. W. *TrAC Trends Anal. Chem.* **2019**, *114*, 81−88.
(5) Lin, Y.; Zhou, Q.; Tang, D.; Niessner, R.; Knopp, D. *Anal. Chem.* **2017**, *89*, 5637−5645.
(6) Song, Z.; Fan, G. C.; Li, Z.; Gao, F.; Luo, X. *Anal. Chem.* **2018**, *90*, 10681−10687.
(7) Gao, Y.; Qi, H.; Shang, M.; Zhang, J.; Yan, J.; Song, W. *Biosens. Bioelectron.* **2019**, *146*, No. 111741.
(8) Fan, G. C.; Shi, X. M.; Zhang, J. R.; Zhu, J. J. *Anal. Chem.* **2016**, *88*, 10352−10356.
(9) Hisatomi, T.; Kubota, J.; Domen, K. *Chem. Soc. Rev.* **2014**, *43*, 7520−7535.
(10) Li, Z.; Yang, H.; Hu, M.; Zhang, L.; Ge, S.; Cui, K.; Yu, J. *ACS Appl. Mater. Interfaces* **2020**, *12*, 17177−17184.
(11) Zhu, Y.; Yan, K.; Xu, Z.; Wu, J.; Zhang, J. *Biosens. Bioelectron.* **2019**, *131*, 79−87.
(12) Dai, W. X.; Zhang, L.; Zhao, W. W.; Yu, X. D.; Xu, J. J.; Chen, H. Y. *Anal. Chem.* **2017**, *89*, 8070−8078.
(13) Wang, G. L.; Liu, K. L.; Shu, J. X.; Gu, T. T.; Wu, X. M.; Dong, Y. M.; Li, Z. J. *Biosens. Bioelectron.* **2015**, *69*, 106−112.
(14) Mikolajczak, D. J.; Berger, A. A.; Koksch, B. *Angew. Chem., Int. Ed.* **2020**, *59*, 8776−8785.
(15) Cao, M.; Sha, L.; Wang, N.; Xu, H.; Cox, H.; Li, R.; Waigh, T.; Han, Y.; Wang, Y.; Lu, J. R. *ACS Appl. Mater. Interfaces* **2019**, *11*, 16357−16366.
(16) Tang, J. D.; Mura, C.; Lampe, K. J. *J. Am. Chem. Soc.* **2019**, *141*, 4886−4899.
(17) Li, K.; Zhang, Z.; Li, D.; Zhang, W.; Yu, X.; Liu, W.; Gong, C.; Wei, G.; Su, Z. *Adv. Funct. Mater.* **2018**, *28*, No. 1801056.
(18) Chin, M.; Tada, S.; Tsai, M. H.; To, Y.; Luo, S. C. *Anal. Chem.* **2020**, *92*, 11260−11267.
(19) Zhang, K.; Fan, Z.; Weng, J.; Zhao, J.; Wang, J.; Wu, H.; Xie, M.; Zhou, H.; Li, H. *ACS Sens.* **2019**, *4*, 2671−2678.
(20) Bahadur, K. C. T.; Tada, S.; Zhu, L.; Uzawa, T.; Minagawa, N.; Luo, S. C.; Zhao, H.; Yu, H.; Aigaki, T.; Ito, Y.; Uzawa, T.; Minagawa, N.; Luo, S. C.; Zhao, H.; Yu, H.; Aigaki, T.; Ito, Y. *Chem. Commun.* **2018**, *54*, 5201−5204.
(21) Jiang, C.; Wang, G.; Hein, R.; Liu, N.; Luo, X.; Davis, J. *Chem. Rev.* **2020**, *120*, 3852−3889.
(22) Wang, G.; Su, X.; Xu, Q.; Xu, G.; Lin, J.; Luo, X. *Biosens. Bioelectron.* **2018**, *101*, 129−134.
(23) Beyer, C. D.; Reback, M. L.; Heinen, N.; Thavalingam, S.; Rosenhahn, A.; Metzler-Nolte, N. *Langmuir* **2020**, *36*, 10996−11004.
(24) Ye, H.; Wang, L.; Huang, R.; Su, R.; Liu, B.; Qi, W.; He, Z. *ACS Appl. Mater. Interfaces* **2015**, *7*, 22448−22457.
(25) Lund, H.; Løvsletten, K.; Paus, E.; Halvorsen, T. G.; Reubsaet, L. *Anal. Chem.* **2012**, *84*, 7926−7932.
(26) Viet, N. X.; Chikae, M.; Ukita, Y.; Maehashi, K.; Matsumoto, K.; Tamiya, E.; Viet, P. H.; Takamura, Y. *Biosens. Bioelectron.* **2013**, *42*, 592−597.
(27) Kang, D.; Hill, J. C.; Park, Y.; Choi, K. S. *Chem. Mater.* **2016**, *28*, 4331−4340.
(28) Li, J. T.; Cushing, S. K.; Zheng, P.; Senty, T.; Meng, F. K.; Bristow, A. D.; Manivannan, A.; Wu, N. Q. *J. Am. Chem. Soc.* **2014**, *136*, 8438−8449.
(29) Sharma, G.; Zhao, Z.; Sarker, P.; Nail, B. A.; Wang, J.; Huda, M. N.; Osterloh, F. E. *J. Mater. Chem. A* **2016**, *4*, 2936−2942.
(30) Patil, R.; Kelkar, S.; Naphade, R.; Ogale, S. *J. Mater. Chem. A* **2014**, *2*, 3661−3668.
(31) Patra, B. K.; Khilari, S.; Pradhan, D.; Pradhan, N. *Chem. Mater.* **2016**, *28*, 4358−4366.
(32) Yu, X.; Shavel, A.; An, X.; Luo, Z.; Ibanez, M.; Cabot, A. *J. Am. Chem. Soc.* **2014**, *136*, 9236−9239.
(33) Dutta, S. K.; Mehetor, S. K.; Pradhan, N. *J. Phys. Chem. Lett.* **2015**, *6*, 936−944.
(34) Fan, G. C.; Zhao, H.; Ma, L.; Lu, Y.; Luo, X. *Chem. Commun.* **2020**, *56*, 1345−1348.
(35) Ding, X.; Yang, K. L. *Anal. Chem.* **2013**, *85*, 10710−10716.
(36) Chang, C. C.; Chen, C. P.; Lee, C. H.; Chen, C. Y.; Lin, C. W. *Chem. Commun.* **2014**, *50*, 14443−14446.
(37) Chang, P. H.; Weng, C. C.; Li, B. R.; Li, Y. K. *Biosens. Bioelectron.* **2020**, *151*, No. 111969.
(38) Hwang, H. J.; Ryu, M. Y.; Park, C. Y.; Ahn, J.; Park, H. G.; Choi, C.; Ha, S. D.; Park, T. J.; Park, J. P. *Biosens. Bioelectron.* **2017**, *87*, 164−170.
(39) Chen, S.; Cao, Z.; Jiang, S. *Biomaterials* **2009**, *30*, 5892−5896.
(40) Nowinski, A. K.; Sun, F.; White, A. D.; Keefe, A. J.; Jiang, S. *J. Am. Chem. Soc.* **2012**, *134*, 6000−6005.
(41) Liu, B.; Liu, X.; Shi, S.; Huang, R.; Su, R.; Qi, W.; He, Z. *Acta Biomater.* **2016**, *40*, 100−118.
(42) Molino, P. J.; Yang, D.; Penna, M.; Miyazawa, K.; Knowles, B. R.; MacLaughlin, S.; Fukuma, T.; Yarovsky, I.; Higgins, M. J. *ACS Nano* **2018**, *12*, 11610−11624.
(43) Roushani, M.; Valipour, A. *Sens. Actuators B Chem.* **2016**, *222*, 1103−1111.
(44) Cao, L.; Fang, C.; Zeng, R.; Zhao, X.; Jiang, Y.; Chen, Z. *Biosens. Bioelectron.* **2017**, *92*, 87−94.
(45) Chiu, N. F.; Kuo, C. T.; Lin, T. L.; Chang, C. C.; Chen, C. Y. *Biosens. Bioelectron.* **2017**, *94*, 351−357.
(46) Chen, H.; Crum, M.; Chavan, D.; Vu, B.; Kourentzi, K.; Willson, R. C. *ACS Appl. Mater. Interfaces* **2018**, *10*, 31845−31849.
(47) Guo, Y.; Zhou, Y.; Xiong, S.; Zeng, L.; Huang, X.; Leng, Y.; Xiong, Y. *Sens. Actuators B Chem.* **2020**, *305*, No. 127439.
(48) Dąbrowski, M.; Ziminska, A.; Kalecki, J.; Cieplak, M.; Lisowski, W.; Maksym, R.; Shao, S.; D'Souza, F.; Kuhn, A.; Sharma, P. S. *ACS Appl. Mater. Interfaces* **2019**, *11*, 9265−9276.

https://dx.doi.org/10.1021/acs.analchem.0c05234
Anal. Chem. 2021, 93, 2706−2712